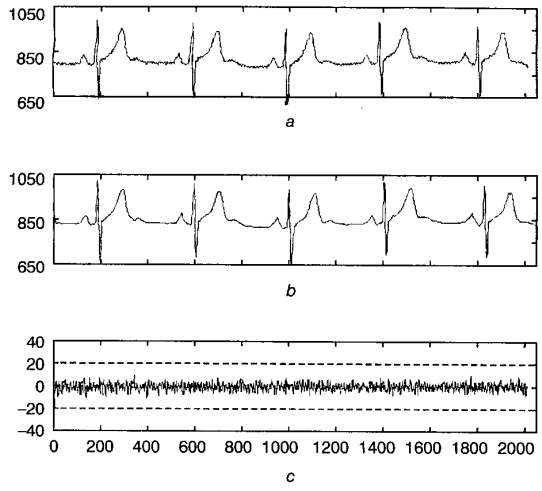

Fig. 1 *Compression of 117 record*
a Original signal
b Reconstructed signal
c Resulting error

Table 1: Evolution of CR and PRD according to variation of PWCZ

PWCZ [%]	80	85	90	91	92	93	94
CR	7.05	8.28	10.89	11.62	12.46	13.49	14.74
PRD	2.64	2.88	3.46	3.73	4.15	4.80	5.76

Table 2: Comparison between obtained results with those of other methods

Methods	Signals	CR	PRD (%)	PWCZ (%)
Proposed method	117	16.24:1	2.5518	95
	119	17.43:1	5.1268	95
	232	9.04:1	0.2981	88
LU, (SPIHT) [1]	117	8:1	1.18	–
	119	21.6:1	5	–
Hilton [4]	117	8:1	2.6	–
Djohn [1]	117	8:1	3.9	–
Rajoub [2]	117	10.7996:1	0.4808	–
	232	4.3141:1	0.3005	–

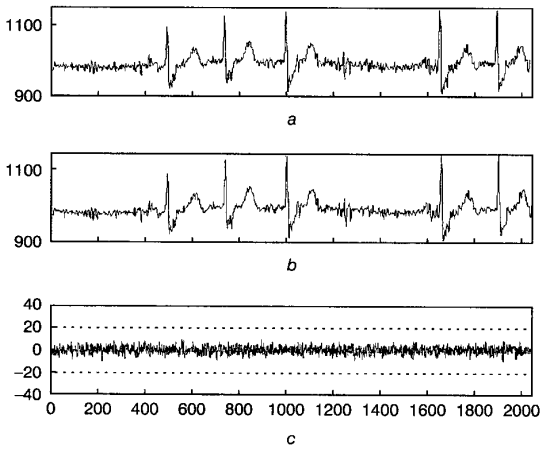

Fig. 2 *Compression of 232 record*
a Original signal
b Reconstructed signal
c Resulting error

The evolution of the average CR and the average PRD of the proposed method, according to the variation of the PWCZ from 80 to 94% is shown in Table 1. The corresponding test dataset [1] is: 100, 101, 102, 103, 107, 109, 111, 115, 117, 118 and 119.

The comparison between the proposed method and the other developed methods is given in Table 2. To compare the results with those in [2], the original and the reconstructed signals with the corresponding resulting error of the 232 record are shown in Fig. 2.

The reconstructed signal is obtained with: ($CR = 9.04{:}1$ and $PRD = 0.2981$). The corresponding PWCZ and TH are: 88% and 10.2997, respectively. For the 117 record, the results are: ($CR = 13.18{:}1$, $PRD = 0.3750$). For the two records, the results obtained are better than in [2]. It is noted that the evaluation is carried out with the PRD calculation in the same way as in [2]. The results of the developed method also outperform those of Hilton [4] and those of Djohn (as reported in [1]).

Conclusion: This study illustrates the effect of the thresholding on the compression ratio and the quality of reconstructed signals. The dichotomy algorithm allows obtaining the PWCZ with the desired precision down to 0.01% for few iterations, therefore the compression ratio can be efficiently controlled.

9 April 2003
Electronics Letters Online No: 20030560
DOI: 10.1049/el:20030560

R. Benzid, M. Benyoucef and D. Arar (*Faculty of Engineering, Department of Electronics, University of Batna, 05000, Algeria*)

E-mail: rbenzid@lycos.com

F. Marir (*Faculty of Engineering, Department of Electronics, University of Constantine, 25000, Algeria*)

M. Boussaad (*Faculty of Science, Department of Mathematics, University of Batna, 05000, Algeria*)

References

1 LU, Z., KIM, D.Y., and PEARLMAN, W.A.: 'Wavelet compression of ECG signals by the set partitioning in hierarchical trees algorithm', *IEEE Trans. Biomed. Eng.*, 2000, **47**, (7), pp. 849–856
2 RAJOUB, B.A.: 'An efficient coding algorithm for the compression of ECG signals using the wavelet transform', *IEEE Trans. Biomed. Eng.*, 2002, **49**, (4), pp. 355–362
3 ISTEPANIAN, R.S.H., and PETROSIAN, A.A.: 'Optimal zonal wavelet-based ECG data compression for a mobile telecardiograpy system', *IEEE Trans. Inf. Technol. Biomed.*, 2000, **4**, (3), pp. 200–211
4 HILTON, M.L.: 'Wavelet and wavelet packet compression of electrocardiograms', *IEEE Trans. Biomed. Eng.*, 1997, **44**, pp. 394–402
5 AHMED, S.M., AL-SHROUF, A., and ABO-ZAHAD, M.: 'ECG data compression using optimal non-orthogonal wavelet transform', *Med. Eng. Phys.*, 2000, **22**, pp. 39–46
6 OLMOS, S., GARCIA, J., JANE, R., and LAGUNA, P.: 'ECG signal compression plus noise filtering with truncated orthogonal expansions', *Signal Process.*, 1999, **79**, pp. 97–115
7 PROVAZNIK, I., and KOZUMPLIK, J.: 'Wavelet transform in electrocardiography-data compression', *Int. J. Med. Inform.*, 1997, **45**, pp. 111–128
8 DONOHO, D.L., JOHNSTONE, I.M., KERKYACHARIAN, G., and PICARD, D.: 'Wavelet shrinkage-asymptopia', *J. R. Stat. Soc. B*, 1995, **57**, pp. 301–369

Chaos in pulse-excited resonator with self feedback

A.S. Elwakil and S. Özoguz

A novel nonautonomous chaotic oscillator based on an active series LC resonator is reported. Excitation is provided by a bipolar pulse-train voltage-source and self feedback via a comparator is employed. The high-dimensional nature of the oscillator is clarified.

Introduction: Nonautonomous chaotic oscillators form a class of circuits which produce chaos when excited by a time-varying source. While there are many known autonomous chaotic oscillators (see [1]), relatively few nonautonomous chaotic oscillators have been

introduced in the literature [2–4]. It is seen from [2–4] that a sinusoidal voltage-source is usually used as the driving force. The amplitude and frequency of this sinusoid both contribute to the chaotic dynamics, as shown in [5], where the effect of excitation on Chua's circuit is studied. Interest in studying the chaotic behaviour of oscillators excited by a bipolar pulse-train has developed recently [6] motivated primarily by behavioural models of neural networks [7, 8].

In [9], it was shown that the third-order passive structure of Chua's circuit, when excited by a periodic pulse-train, can exhibit multiple-scroll chaos. In this Letter, we show that an active second-order LC resonator can also exhibit chaos when excited by a periodic pulse-train. Nonlinearity in this case is provided by a comparator (or digital inverter), employed to provide self feedback to the excited node with output voltage levels similar to those of the pulse-train.

Pulse-excited LC resonator: Consider the circuit shown in Fig. 1 which comprises a series LC resonator, activated by means of a current-controlled linear negative resistor ($-r$), an opamp operating as a comparator and a periodic pulse-train voltage source V_P. The output voltage levels of V_P and the comparator are both equal to $\pm V_{cc}$, which are also the dual DC supplies of the whole circuit (including the negative resistor). The comparator output voltage V_F depends on the voltage across the capacitor V_C and is given by:

$$V_F = V_{cc}\text{sgn}(V_C) \tag{1}$$

while the periodic pulse-train V_P is given by:

$$V_P = V_{cc}\text{sgn}(\sin(\omega_P t)) \tag{2}$$

where ω_P is the oscillation frequency.

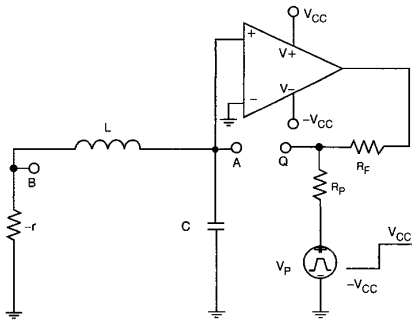

Fig. 1 *Proposed pulse-excited LC resonator with self feedback*

At the node labelled Q, the effect of the driving force V_P and the comparator output V_F are added together after being converted into weighted currents through resistors R_P and R_F, respectively. The combined excitation at node Q can either be applied to internal node A or internal node B. In the Q–A connection mode, the circuit is described by the following two differential equations:

$$C\dot{V}_C = \frac{V_P - V_C}{R_P} + \frac{V_F - V_C}{R_F} - I_L \tag{3a}$$

$$L\dot{I}_L = V_C + rI_L \tag{3b}$$

where V_F and V_P are given respectively by (1) and (2). By defining the dimensionless variables: $X = V_C/V_{cc}$, $Y = rI_L/V_{cc}$, $\tau = t/\sqrt{(LC)}$, $\alpha = \sqrt{(L/C)}/r$, $\beta = r/R_P$, $\gamma = r/R_F$ and $\phi = \omega_P\sqrt{(LC)}$, the previous equations transform into:

$$\dot{X} = \alpha[-Y - (\beta + \gamma)X + \gamma f(X) + \beta p(\tau)] \tag{4a}$$

$$\alpha\dot{Y} = X + Y \tag{4b}$$

where $f(X)$ and $p(\tau)$ are given respectively as:

$$f(X) = \text{sgn}(X) = \begin{cases} 1 & X \geq 0 \\ -1 & X < 0 \end{cases} \tag{5}$$

$$p(\tau) = \text{sgn}(\sin(\phi\tau)) = \begin{cases} 1 & \sin(\phi\tau) \geq 0 \\ -1 & \sin(\phi\tau) < 0 \end{cases} \tag{6}$$

The strength of excitation of the pulse-train and the self feedback comparator are quantified via the two parameters β and γ respectively.

Numerical integration of the system using an adaptive-step Runge-Kutta algorithm was performed after taking $\alpha = 50$, $\beta = \gamma = 1$ and $\phi = 0.1$. The chaotic attractor projection in the X–Y plane is shown in Fig. 2. A positive Lyapunov exponent equal to $+0.1523$ was calculated. It is clear that (4) has four equilibrium points; two in the region $X > 0$ given by $(x_0, y_0) = [(\gamma \pm \beta)/(\gamma + \beta - 1)](1, -1)$ and two in the region $X < 0$ given by $(x_0, y_0) = [(-\gamma \pm \beta)/(\gamma + \beta - 1)](1, -1)$. The special case $\beta = \gamma$ implies that two of these equilibria coincide with the origin $(0, 0)$. The eigenvalues at all points are identical since $f(X)$ and $p(\tau)$ only affect the position of the equilibrium point but do not contribute to the state-transition matrix.

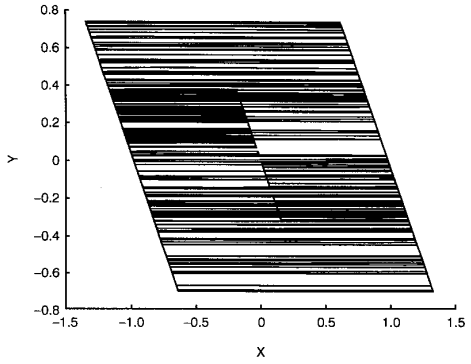

Fig. 2 *Chaotic X–Y phase space of circuit in Q–A connection mode*

It is well known that for a linear system to sustain sinusoidal oscillations, it must be at least of second-order. The simplest such system is given by:

$$\ddot{Z} + \phi^2 Z = 0 \tag{7}$$

which yields $Z(\tau) = \sin(\phi\tau)$. Using this sinusoidal waveform in conjunction with a comparator, a pulse-train is obtained, as modelled by (6). Therefore, one can rewrite the differential equations describing the circuit in the following form:

$$\dot{X} = \alpha[-Y - (\beta + \gamma)X + \gamma f(X) + \beta f(Z)] \tag{8a}$$

$$\alpha\dot{Y} = X + Y \tag{8b}$$

$$\ddot{Z} = -\phi^2 Z \tag{8c}$$

with $f(X) = \text{sgn}(X)$ and $f(Z) = \text{sgn}(Z)$. Hence, the second-order non-autonomous system (4) has been transformed into a fourth-order autonomous system which evidently admits chaos. Numerical integration of (8) when performed with $\alpha = 50$, $\beta = \gamma = 1$, $\phi = 0.1$ and $Z(0) = 1$ show results identical to those plotted in Fig. 2. However, it is now possible to construct the three-dimensional view of the chaotic attractor, shown in Fig. 3, in the X–Y–Z subspace.

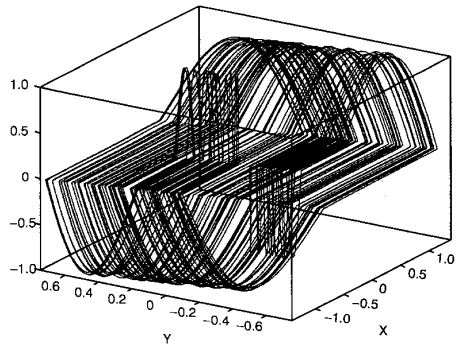

Fig. 3 *3-D view of chaotic attractor in Q–A connection mode*

In the Q–B node connection (see Fig. 1), the linear negative resistor cannot remain current-controlled and has to be voltage-controlled; the

control voltage is held on any parasitic capacitor C_P in parallel with this resistor. Therefore, the structure is third-order and is described by:

$$\dot{X} = -\alpha Y \tag{9a}$$

$$\alpha\dot{Y} = X - Z \tag{9b}$$

$$\varepsilon\dot{Z} = \alpha[Y - (\beta + \gamma - 1)Z + \gamma f(X) + \beta p(\tau)] \tag{9c}$$

where the same dimensionless variables in (4) are used in addition to $Z = V_{CP}/V_{cc}$ and $\varepsilon = C_P/C$. The four equilibrium points of (9) are $(x_0, y_0, z_0) = [(\pm\beta \pm \gamma)/(\beta + \gamma - 1)](1, 0, 1)$ and the chaotic attractor observed when numerically integrating (9) with $\alpha = \phi = 0.1$, $\beta = \gamma = 200$, and $\varepsilon = 0.001$ is similar to that observed in the pulse excited Chua's circuit studied in [9]. It is also possible to transform this third-order nonautonomous system into a fifth-order autonomous system, as described above.

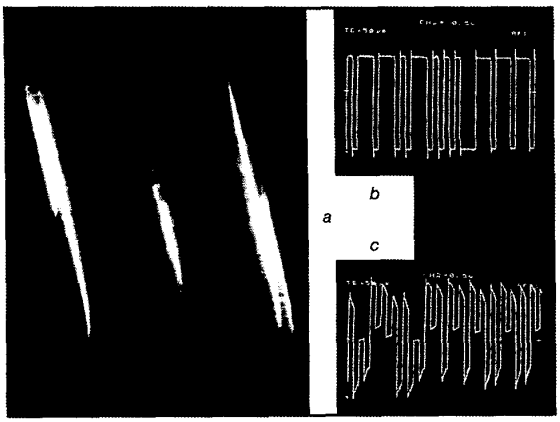

Fig. 4 *Experimental observation in Q–A connection mode*
a V_C–I_L phase space (*X*-axis: 0.5 V/div; *Y*-axis: 1 V/div)
b Sample comparator output V_F
c V_C time waveform (*X*-axis: 0.5 μs/div; *Y*-axis: 0.5 V/div)

Experimental results: The circuit of Fig. 1 was constructed using discrete components. The floating inductor and the negative resistor were both actively simulated using AD844 current feedback opamps (CFOAs). Since the results in the *Q–B* connection mode are similar to those reported in [9], results of the *Q–A* excitation mode only are shown. The used component values were: $L = 40$ mH, $r = R_F = R_P = 2.2$ kΩ and $C = 4.7$ pF and the frequency of the pulse-train was $f = 38$ kHz. These values correspond to $\alpha = 41.9$, $\beta = \gamma = 1$ and $\phi = 0.104$. In Fig. 4, the observed V_C–I_L trajectory is shown along with the time waveforms of V_F and V_C, respectively.

Conclusion: A pulse-excited series LC resonator was shown to exhibit chaos. The circuit can be considered as a periodic-to-chaotic pulse-train transformer by considering V_P as the input clock and V_F as the output sequence.

Acknowledgment: This work has been supported by the Turkish Academy of Sciences, in the framework of the Young Scientist Award Program (İSÖ/TÜBA-GEBİP/2002-1-16).

24 February 2003
Electronics Letters Online No: 20030559
DOI: 10.1049/el:20030559

A.S. Elwakil (*Department of Electrical and Electronic Engineering, University of Sharjah, P.O. Box 27272, Sharjah, United Arab Emirates*)

S. Özoguz (*Faculty of Electrical-Electronics Engineering, Istanbul Technical University 80626, Maslak, Istanbul, Turkey*)

References

1 ELWAKIL, A.S., and KENNEDY, M.P.: 'Construction of classes of circuit-independent chaotic oscillators using passive-only nonlinear devices', *IEEE Trans. Circuits Syst. I*, 2001, **48**, pp. 289–307
2 AZZOUZ, A., DUHR, R., and HASLER, M.: 'Transition to chaos in a simple non-linear circuit driven by a sinusoidal voltage source', *IEEE Trans. Circuits Syst. I*, 1983, **30**, pp. 913–914
3 MURALI, K., LAKSHMANAN, M., and CHUA, L.O.: 'The simplest dissipative nonautonomous chaotic circuit', *IEEE Trans. Circuits Syst. I*, 1994, **41**, pp. 462–463
4 LACY, J.G.: 'A simple piece-wise-linear nonautonomous circuit with chaotic behaviour', *Int. J. Bifurcation Chaos Appl. Sci. Eng.*, 1996, **6**, pp. 2097–2100
5 MURALI, K., and LAKSHMANAN, M.: 'Effect of sinusoidal excitation on Chua's circuit', *IEEE Trans. Circuits Syst. I*, 1992, **39**, pp. 264–270
6 MITSUBORI, K., and SAITO, T.: 'Mutually pulse-coupled chaotic circuits by using dependent switched capacitors', *IEEE Trans. Circuits Syst. I*, 2000, **47**, pp. 1469–1478
7 NAKANO, H., and SAITO, T.: 'Basic dynamics from an integrate and-fire chaotic circuits with a periodic input', *IEICE Trans. Fundam. Electron. Commun. Comput. Sci.*, 2001, **E84**, pp. 1293–1300
8 AIHARA, K.: 'Chaos engineering and its applications to parallel distributed processing with chaotic neural networks', *Proc. IEEE 90*, 2002, pp. 919–930
9 ELWAKIL, A.S.: 'Nonautonomous pulse-driven chaotic oscillator based on Chua's circuit', *Microelectron. J.*, 2002, **33**, pp. 479–486

Performance analysis of optimised CMOS comparator

H.P. Le, A. Zayegh and J. Singh

A high-speed low-power latched CMOS comparator circuit is presented. Demonstrated is a circuit optimisation technique to obtain minimum offset error at 500 MHz sampling speed. Also, a mathematical model representing the noise in the device is developed. After optimisation, the comparator achieved 10-bit resolution on a 1 V differential input at 500 MHz speed and had a noise figure of 4.747 dB at this frequency.

Introduction: High-speed low-power analogue-to-digital converters (ADCs) are the critical building blocks for modern communication and signal processing systems [1]. In any ADC, comparators are the most critical components because their input offset voltage, delay and input range directly influence the resolution and speed of the ADC. Therefore, there is a continued search for architectures and circuit techniques enabling comparators to attain faster speed with minimum offset error and power dissipation. There are many comparators that have been successfully designed [2–4]. However, they have not achieved a sampling speed beyond 200 MHz with 10 bit of resolution. Furthermore, the noise generated within a comparator itself plays an important role in its overall performance at high frequencies. Therefore, a model that can accurately predict the device noise characteristics, is crucial.

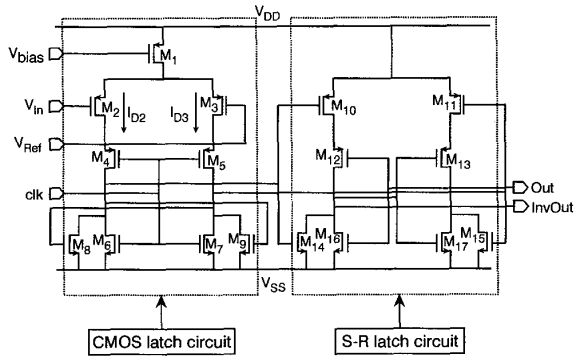

Fig. 1 *Schematic diagram of latched comparator*

Comparator design: The proposed comparator consists of a CMOS latch circuit and an S-R latch circuit, as shown in Fig. 1. The comparator was designed using fully CMOS technology, which produces eligible leakage current when the comparator is in recharge mode. Moreover, the differential pair directly controls the currents feeding to